

The Abundance Pattern of O, Ne, Mg, and Fe in the Interstellar Medium of S0 Galaxy NGC 4382 Observed with Suzaku

Ryo NAGINO and Kyoko MATSUSHITA

Tokyo University of Science, 1-3 Kagurazaka, Shinjyuku-ku, Tokyo, Japan, 162-8601
nagino@rs.kagu.tus.ac.jp; matusita@rs.kagu.tus.ac.jp

(Received 2009 November 4; accepted 2010 April 14)

Abstract

We derived O, Ne, and Mg abundances in the interstellar medium (ISM) of a relatively isolated S0 galaxy, NGC 4382, observed with the Suzaku XIS instruments and compared the O/Ne/Mg/Fe abundance pattern to those of the ISM in elliptical galaxies. The derived temperature and Fe abundance in the ISM are about 0.3 keV and 0.6–2.9 solar, respectively. The abundance ratios are derived with a better accuracy than the abundances themselves: O/Fe, Ne/Fe, and Mg/Fe ratios are 0.3, 0.7, and 0.6, respectively, in solar units. The O/Fe ratio is smaller than that of the ISM in elliptical galaxies, NGC 720, NGC 1399, NGC 1404, and NGC 4636, observed with Suzaku. Since O, Ne, and Mg are predominantly synthesized by supernovae (SNe) of type II, the observed abundance pattern indicates that the contribution of SN Ia products is higher in the S0 galaxy than in the elliptical galaxies. Since the hot ISM in early-type galaxies is an accumulation of stellar mass and SN Ia products, the low O/Fe ratio in the ISM of NGC 4382 reflects a higher rate of present SNe Ia, or stars containing more SN Ia products than those in elliptical galaxies.

Key words: galaxies: individual (NGC 4382), galaxies: ISM, galaxies: abundances, X-rays: ISM

1. Introduction

Early-type galaxies have a hot, X-ray emitting interstellar medium (ISM), which is considered to be gravitationally confined (e.g., Forman et al. 1985; Mathews & Brighenti 2003). X-ray observations of the metal abundances in the ISM of early-type galaxies provide a key to understanding the history of star formation and the evolution of galaxies, because the metals in the ISM come from type Ia supernovae (SNe Ia) and stellar mass loss.

A lot of observational evidence suggests that a significant fraction of present early-type galaxies have transformed from late-type galaxies (e.g., Dressler et al. 1997; Fasano et al. 2000; Treu et al. 2003; Postman et al. 2005; Smith et al. 2005). From $z \sim 0.5$, the fraction of S0 galaxies in clusters of galaxies has increased, whereas, that of spirals has decreased, with no evolution in the fraction of ellipticals (Kodama et al. 2004; Desai et al. 2007). Poggianti et al. (2009) found that these changes appear more strongly in less massive clusters with lower velocity dispersion. These results suggest that spiral galaxies changed into S0 galaxies at $z < 0.5$, falling into clusters of galaxies. The metallicity of stars in galaxies reflects in the star formation history, therefore, it is an important parameter for understanding the evolution of galaxies.

Optical observations indicate that Mg/Fe and α /Fe ratios of stars are super-solar in the cores of bright early-type galaxies and increases with galactic mass (e.g., Faber et al. 1992; Worthey et al. 1992; Nelan et al. 2005; Thomas et al. 2005; Graves et al. 2007). This overabundance of Mg relative to Fe is the key indicator that galaxy formation occurred before a substantial number of SNe Ia could explode and contribute to lowering the these ratios

(e.g., Bernardi et al. 2003; Nelan et al. 2005; Smith et al. 2006; Graves et al. 2007; Pipino et al. 2009). However, absorption-line indices that account for abundance ratios also depend on the age distribution of stars. Optical spectroscopy is limited within the very center of galaxies.

Using X-ray observations, we can directly determine the metal abundances of the ISM, and constrain the stellar metallicity of the entire galaxy. The atomic data for lines at X-ray wavelengths are simpler than for those in optical spectra, and the structure of the hot ISM is also much simpler than stellar population data. Therefore, we can estimate the temperature and metallicity of the hot ISM through X-ray spectra with small systematic uncertainties. XMM-Newton EPIC and RGS provided the means to measure O and Mg abundances in some systems, but reliable results have been obtained only for several central galaxies in groups and clusters (e.g., Xu et al. 2002; Matsushita et al. 2003; Tamura et al. 2003; Matsushita et al. 2007a). The ISM in such regions might be polluted by the gas of clusters or groups (e.g., Matsushita 2001; Matsushita et al. 2002; Nagino & Matsushita 2009).

With the Suzaku X-ray satellite, O, Ne, and Mg abundances of four elliptical galaxies, NGC 720 (Tawara et al. 2008), NGC 1399 and NGC 1404 (Matsushita et al. 2007b), and NGC 4636 (Hayashi et al. 2009), have been measured. The XIS detector onboard Suzaku (Mitsuda et al. 2007) can constrain O, Ne, and Mg abundances well because its energy resolution is better, and its background is lower than any previous X-ray CCD detector (Koyama et al. 2007). According to the new solar abundance table of Lodders (2003), the abundance ratios of these elliptical galaxies are close to the solar values. Assuming the SN II

abundance pattern of Iwamoto et al. (1999), about 80% of Fe is synthesized by SNe Ia (Matsushita et al. 2007b).

The abundance pattern of the hot ISM in S0 galaxies observed with Suzaku has not been reported. In this paper, we present the temperature and abundances of O, Ne, Mg, and Fe in the ISM within $4 r_e$ of the S0 galaxy NGC 4382, observed with Suzaku. Here, r_e is the effective radius of the galaxy. For NGC 4382, r_e corresponds to 0.91 arcmin (de Vaucouleurs et al. 1991). The distance to NGC 4382 is 16.8 Mpc (Tully 1988), and its redshift, $z=0.002432$, is taken from the NASA/IPAC extragalactic database (NED). NGC 4382 is located in the outskirts of the Virgo cluster, 1.7 Mpc from cD galaxy M87. The central stellar velocity dispersion of the galaxy, 179 km s^{-1} and its $[\alpha/\text{Fe}]$ value, 0.12 ± 0.06 (McDermid et al. 2006), are much smaller than those of the four elliptical galaxies, observed with Suzaku. These values were derived only within two arcsec of the center of NGC 4382, and we do not know the metallicity of stars outside of the central region. So far, NGC 4382 has been observed with ROSAT (Fabbiano et al. 1994), ASCA (Kim et al. 1996), Chandra (Sivakoff et al. 2003; Athey 2007) and XMM-Newton (Sansom et al. 2006; Nagino & Matsushita 2009). These X-ray observations suggest that the temperature of the ISM in NGC 4382 is about 0.3–0.4 keV, which is much lower than those of the four early-type galaxies observed with Suzaku. Since no the intracluster medium (ICM) around NGC 4382 has been detected, this galaxy is suitable for investigating heavy elements in the ISM of the galaxy itself.

Throughout this paper, we use a Hubble constant of $H_0 = 70 \text{ km s}^{-1} \text{ Mpc}^{-1}$. We adopt the new solar abundance table of Lodders (2003). The abundances of O and Fe have increased by about 70% and 60%, respectively. Unless otherwise specified, errors are quoted at 90% confidence.

2. Observation and data reduction

Suzaku observed NGC 4382 in June 2008 with an exposure of 99 ksec in the XIS nominal position, pointing at the center of NGC 4382. Figure 1 shows a 0.3–2.0 keV image of NGC 4382. We analyzed only the XIS data in this paper, although Suzaku observations were performed with both XIS and HXD. The XIS instrument consists of three sets of X-ray CCDs (XIS0, 1, and 3). XIS1 is a back-illuminated (BI) sensor, while XIS0 and 3 are front-illuminated (FI) ones. In this observation, these instruments were operated in the normal clocking mode (8 s exposure per frame), with the standard 5×5 or 3×3 editing mode.

Our analysis was performed using XSPEC version 11.3.2ag and HEASoft version 6.6.2. We processed the XIS data with `xispi`, using the calibration files distributed on 04-03-2009. Then, we cleaned the XIS data by assuming thresholds of $> 5^\circ$ on the Earth elevation angle, and $> 20^\circ$ on the day-earth elevation angle. The total exposure time for both FI and BI sensors amounts to ~ 99 ksec after standard data screening. Event screening with cut-off rigidity

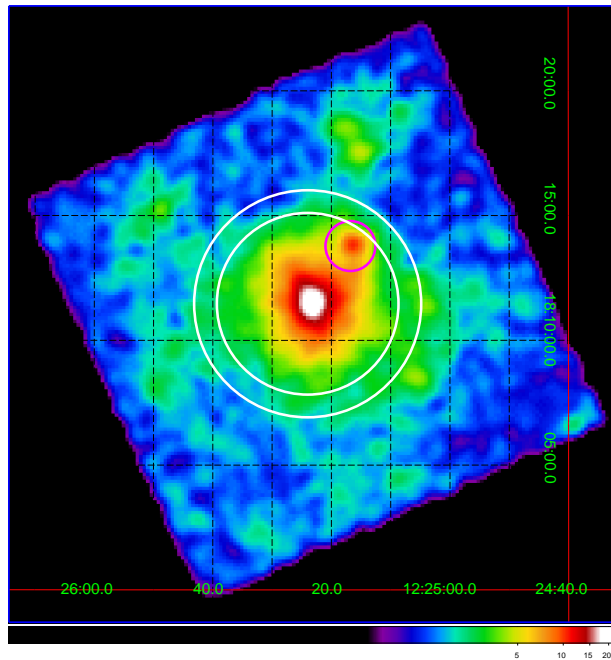


Fig. 1. Raw XIS image of NGC 4382 within an energy range of 0.3–2.0 keV. XIS0, 1, and 3 images were added in sky coordinates. Non-X-ray background (NXB) and cosmic X-ray background (CXB) were not subtracted. Image was smoothed with a Gaussian of $\sigma = 0.56$ arcmin. White circles represent regions within $4 r_e$ and $5 r_e$, respectively. Point source indicated by magenta circle is excluded from spectra.

(COR) was not performed on our data.

XIS response files were calculated using the `xisrmfgen` response matrix file (RMF) generator (Ishisaki et al. 2007), version 02-28-2009. Ancillary response files (ARF) were calculated using `xissimarfgen`, version 01-08-2009, assuming flat-sky emission. We note that ARF files assuming a point-source, a β -model profile, or flat-sky are almost the same within the energy range of 0.4 to 5 keV, except for normalization. Slight degradation of the energy resolution was considered in the RMF, and a decrease in the low-energy transmission of the XIS optical blocking filter (OBF) was included in the ARFs. To subtract the contribution of non-X-ray background (NXB), we used `xisnxbgen`, which generates the NXB spectrum from a dark Earth database (Tawa et al. 2008).

3. Spectral analysis

As shown in Figure 1, we extracted the spectra within a $4 r_e$ circle centered on the optical center of NGC 4382 from NED. We also used the region outside $5 r_e$ to estimate the background. Northwest of NGC 4382, a point-like X-ray source was detected at 0.3–2.0 keV. We excluded this source from each spectrum.

We used the spectra from the BI (XIS1) and FI (XIS0 and 3) sensors for the energy ranges of 0.4–5.0 keV and 0.6–5.0 keV, respectively, since subtracting background lines is difficult above 5.0 keV, and the ISM does not emit photons above 5.0 keV. The energy range around

the Si K-edge (1.82–1.84 keV) was ignored as a result of a problem in the response matrix. The remaining total photon counts with XIS0, 1, and 3 are 3490, 6604, and 3617 counts, respectively. Although two calibration sources emitting strong lines above 5 keV are located at the corners of each XIS, spectral analysis is not affected below 5 keV. Therefore, we included these regions, and analyzed the spectra below 5 keV. The spectra of XIS detectors (XIS0, 1, and 3) were fitted simultaneously with a model consisting of the ISM emission, unresolved discrete sources, cosmic X-ray background (CXB), and Galactic components. Here, the spectra of the NXB were subtracted.

3.1. The ISM component

We adopted a single-temperature ν APEC model (Smith et al. 2001) as the ISM thin thermal emission component (hereafter, the 1T model). The ISM in early-type galaxies originates mainly from stellar mass loss, and most of the metals in these stars are the products of SNe. The metal abundances of He, C, N, and Al were fixed at solar values. We organized the abundances of other heavy elements into five groups: O; Ne; Mg; the Si group (Si, S, Ar, and Ca); and the Fe group (Fe and Ni), and allowed them to vary. This is because significant detections of the ionized O, Ne, Mg, Si, and Fe lines are expected. In this study, we assume that abundances of S, Ar, and Ca are the same as that of Si, taking into account the metal synthesis process in SNe. These lines were not significantly observed, and hence we could not determine the abundance of each line. In our Galaxy, Ni/Fe ratios synthesized from both SN Ia and SN II are solar values (Edvardsson et al. 1993).

This component was subjected to a common absorption with a fixed column density (N_{H}) at the Galactic value of Dickey & Lockman (1990), $2.5 \times 10^{20} \text{cm}^{-2}$.

3.2. Unresolved discrete sources

For unresolved point sources, we added a power-law model, in which the photon index was fixed at 1.6 (Irwin et al. 2003). The power-law model described the total spectra of discrete sources in early-type galaxies well, and was successfully used for this role in previous studies (Blanton et al. 2001; Randall et al. 2004). This component, as well as the ISM component, was also subjected to a common absorption with fixed N_{H} at the Galactic value of Dickey & Lockman (1990).

3.3. CXB and Galactic emission

For the CXB component, we adopted a power-law model with a photon index $\Gamma = 1.4$ (Kushino et al. 2002). Galactic emission arises mainly from the local hot bubble (LHB) and the Milky Way halo (MWH). We used a two-temperature APEC model for these components and fixed the temperatures of the LHB and MWH emission at 0.1 and 0.3 keV, respectively, following previous studies (e.g., Komiyama et al. 2009; Konami et al. 2009; Hayashi et al. 2009; Yamasaki et al. 2009). CXB and MWH components were subjected to absorption at the Galactic value, while the LHB was not.

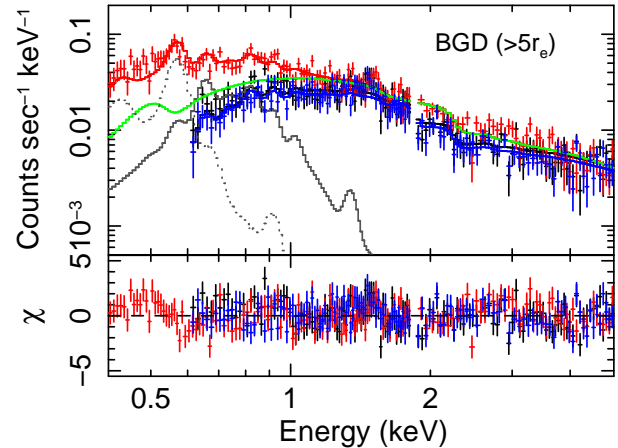


Fig. 2. Spectra outside of $5 r_e$ observed with XIS0 (black), XIS1 (red), and XIS3 (blue). These spectra are fitted with a sum of the CXB and Galactic models. Lower panel shows fit residuals. Here, for simplicity, only model components for the XIS1 spectra are shown. Green and gray lines correspond to CXB and Galactic emission components, respectively.

As shown in Figure 1, we fitted the spectra with the NXB subtracted outside of $5 r_e$ from the center of NGC 4382 to estimate the contribution from the CXB and Galactic emission. In this study, we assumed that there is no emission from the galaxy beyond $5 r_e$. The normalizations of CXB and Galactic components were allowed to vary. Figure 2 shows the best-fit model and spectra for the CXB and Galactic components. The spectra are well described by the model with a reduced- χ^2 value of 1.23; there were 419 degrees of freedom.

3.4. Spectral fitting within $4 r_e$

Next, we fitted the spectra within $4 r_e$ and outside of $5 r_e$ of XIS0, 1, and 3 simultaneously with the 1T model for the ISM, two power-law models for unresolved sources and CXB, and two APEC models for Galactic emission. Here, we assumed that the normalizations of the ISM and unresolved source components were fixed at 0 beyond $5 r_e$. We also assumed that the CXB and Galactic emission within $4 r_e$ and beyond $5 r_e$ have the same surface brightness and spectral parameters. Figure 3 shows the XIS spectra fitted in this way. The derived χ^2 , ISM temperature, and abundances are summarized in Table 1. This fit provides a rather small reduced- χ^2 of ~ 1.15 , although residual structures appear around 0.8 keV.

4. Results

4.1. ISM temperature and abundances

Table 1 summarizes the best-fit parameters of temperature and abundances. The ISM temperature within $4 r_e$ is about 0.3 keV. This temperature is lower than those of early-type galaxies, NGC 720, NGC 1399, NGC 1404, and NGC 4636, which have been observed with Suzaku (Matsushita et al. 2007b; Tawara et al. 2008; Hayashi et al. 2009). This temperature is consistent with those de-

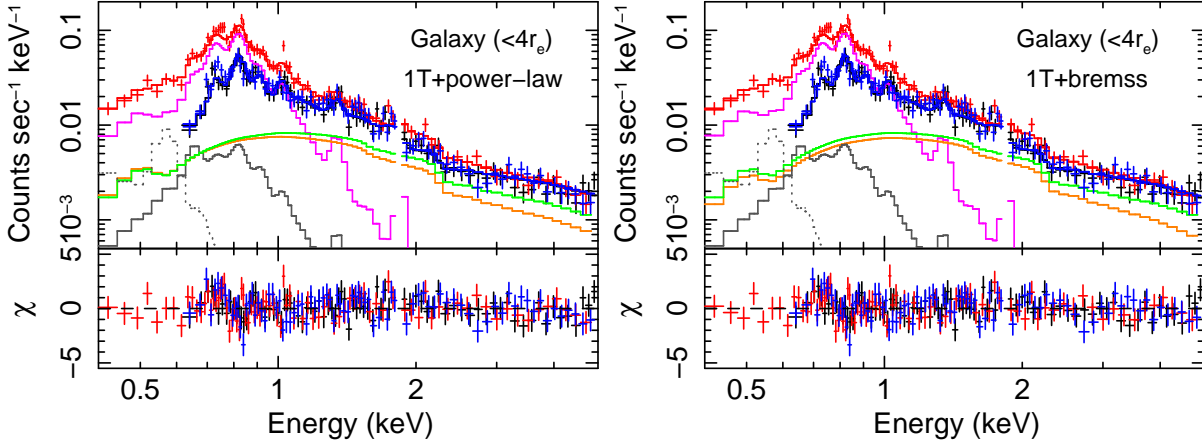


Fig. 3. Spectra within $4 r_e$ observed with XIS0 (black), XIS1 (red), and XIS3 (blue). These spectra are fitted with 1T+power-law (left), and 1T+bremss (right) models. Lower panels show fit residuals. For simplicity, only model components for XIS1 spectra are shown. Magenta and orange lines represent ISM components and unresolved sources, respectively. Green and gray lines correspond to CXB and Galactic emission components, respectively.

Table 1. Results of spectral fittings within $4 r_e$ of NGC 4382 with 1T models

model	kT (keV)	O (solar)	Ne (solar)	Mg (solar)	Fe (solar)	$\chi^2/\text{d.o.f.}$
1T+power-law	$0.311^{+0.024}_{-0.019}$	$0.33^{+0.67}_{-0.16}$	$0.70^{+1.36}_{-0.31}$	$0.63^{+1.29}_{-0.33}$	$1.02^{+1.91}_{-0.43}$	759 / 658
1T+bremss	$0.308^{+0.023}_{-0.018}$	$0.30^{+0.47}_{-0.13}$	$0.64^{+0.95}_{-0.26}$	$0.56^{+0.90}_{-0.28}$	$0.93^{+1.34}_{-0.37}$	754 / 658

model	O/Fe (solar)	Ne/Fe (solar)	Mg/Fe (solar)
1T+power-law	$0.33^{+0.19}_{-0.11}$	$0.69^{+0.15}_{-0.13}$	$0.62^{+0.27}_{-0.27}$
1T+bremss	$0.32^{+0.18}_{-0.10}$	$0.68^{+0.15}_{-0.13}$	$0.60^{+0.27}_{-0.27}$

rived from previous observations with ROSAT (Fabbiano et al. 1994), Chandra (Sivakoff et al. 2003; Athey 2007), and XMM-Newton (Nagino & Matsushita 2009). On the other hand, Sansom et al. (2006) detected a higher ISM temperature of about 0.4 keV with XMM-Newton EPIC.

The abundances are less constrained, and Fe abundance within $4 r_e$ is ~ 0.6 – 2.9 solar with large errors. This value is consistent with those of the early-type galaxies, NGC 720, NGC 1399, NGC 1404, and NGC 4636. The other abundances, O, Ne, and Mg, are mostly consistent with the Fe abundance within large error bars, but tend to have lower values than that of Fe.

4.2. Abundance ratios

Figure 4 shows the confidence contours of O, Ne, and Mg abundances against Fe abundance. Fe in the ISM originates from type Ia and type II SNe, whereas, O, Ne, and Mg come from type II SNe (Iwamoto et al. 1999; Nomoto et al. 2006). Thus, O-, Ne-, and Mg-to-Fe abundance ratios are particularly important for constraining the contributions from type Ia and II SNe. These contours show elongated shapes, especially for the Ne and O abundances vs. Fe abundance, and are along the lines representing constant O/Fe, Ne/Fe, and Mg/Fe ratios. Thus, we can constrain the metal-to-Fe abundance ratios well, although

the individual error bars for each metal abundance are large.

O/Fe, Ne/Fe and Mg/Fe ratios derived from these confidence contours are also summarized in Table 1. Abundance ratios of O/Fe, Ne/Fe, and Mg/Fe in solar units are $0.33^{+0.19}_{-0.11}$, $0.69^{+0.15}_{-0.13}$, and $0.62^{+0.27}_{-0.27}$, respectively. O abundance is especially small relative to the Fe abundance.

4.3. Uncertainties in spectral fit

In this section, we examine the uncertainties in the abundance determination because of an uncertainty in the spectral modeling.

To investigate the systematic effect of the model for unresolved sources, described in Section 3.2, we also fitted the components with a bremsstrahlung model (e.g., Matsushita et al. 1994; Irwin et al. 2000) and compared the results with those using the power-law model. Here, we fixed the temperature of the bremsstrahlung model at 7.0 keV (Matsushita et al. 1994). The best-fit spectra are shown in Figure 3. As shown in Table 1, the derived results are almost the same.

We also tried a spectral fitting with a two-temperature model for the ISM (hereafter, the 2T model). However, the values of reduced- χ^2 did not improve, and the same

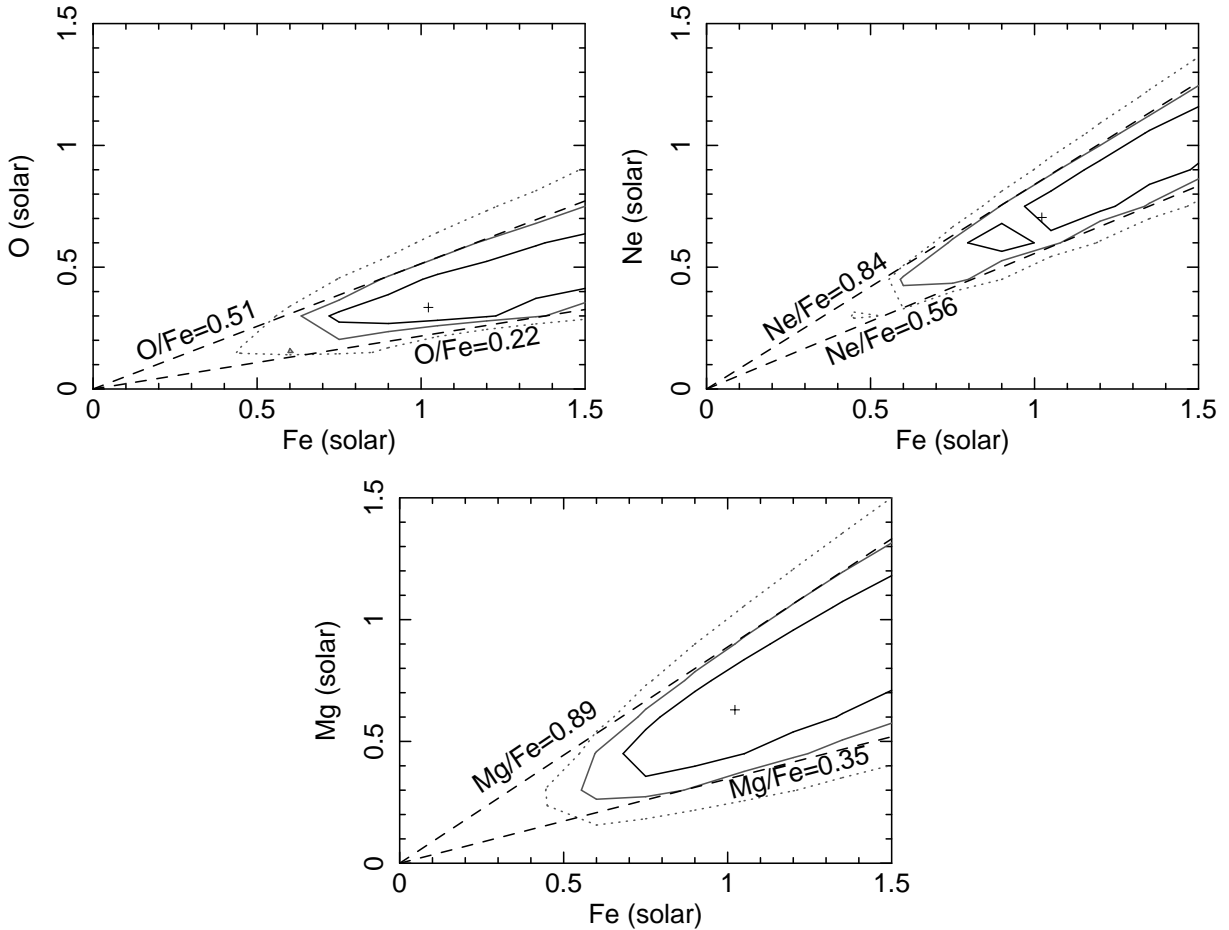


Fig. 4. Confidence contours for O, Ne, and Mg abundances vs. Fe abundance. Crosses denote the best-fit, and black-solid, gray-solid, and gray-dotted contours represent 68%, 90%, and 99% confidence levels, respectively. Dashed lines correspond to constant abundance ratios.

residuals remained around 0.8 keV, at the Fe-L line energies. The temperature of the first component was almost the same as that in the 1T model, and the normalization of the second component was almost zero. Thus, the derived abundances were unchanged. We then fitted the spectra with a five-temperature model for the ISM (hereafter the 5T model); we fixed the ISM temperatures at (i) 0.2, 0.4, 0.6, 0.8, and 1.0 keV and (ii) 0.1, 0.2, 0.3, 0.4, and 0.5 keV.

Figure 5 shows spectra fitted with the 5T(i) and 5T(ii) models. The spectral fitting with the 5T(i) model provided a worse χ^2 value than that with the 1T model (Table 2). Only the normalizations of ISM components with temperatures of 0.2 and 0.4 keV are >0 , and the normalizations of the other ISM components fall to 0. This suggests that temperature components above 0.6 keV do not exist in the ISM of NGC 4382. On the other hand, the spectral fitting with the 5T(ii) model provides the same χ^2 as the 1T model (Table 2). In this fitting, only the normalizations of temperature components at 0.3, 0.4, and 0.5 keV are >0 (cf. Figure 5). The contribution of the 0.3 keV component is the largest of the three temperature components at about 97%. The derived abundances

and abundance ratios did not differ from the results of 1T spectral fitting. These 5T models even gave similar residual structures around 0.8 keV. These discrepancies in the Fe-L energy range are also seen in Suzaku observations of NGC 720, NGC 1404, and NGC 4636, whose ISM temperatures are also ~ 0.6 keV (Matsushita et al. 2007b; Tawara et al. 2008; Hayashi et al. 2009). Therefore, these residual structures are likely to be related to poorly modeled Fe-L lines.

To investigate the effect of the temperatures of the Galactic components on the ISM abundances of NGC 4382, we allowed the temperature of the MWH component to vary and re-fitted the spectra. We got almost the same ISM temperature and abundances.

4.4. Radial profiles

To study radial discrimination, we investigated the spectra extracted from the different radial regions, $R < 2r_e$, $2r_e < R < 4r_e$, and $3r_e < R < 6r_e$. Here, R is the projected radius from the galaxy's center. In Table 3, we summarized the fitting results. A low signal-to-noise ratio does not constrain the abundances. We can derive the abundance ratios against Fe only, although each value has

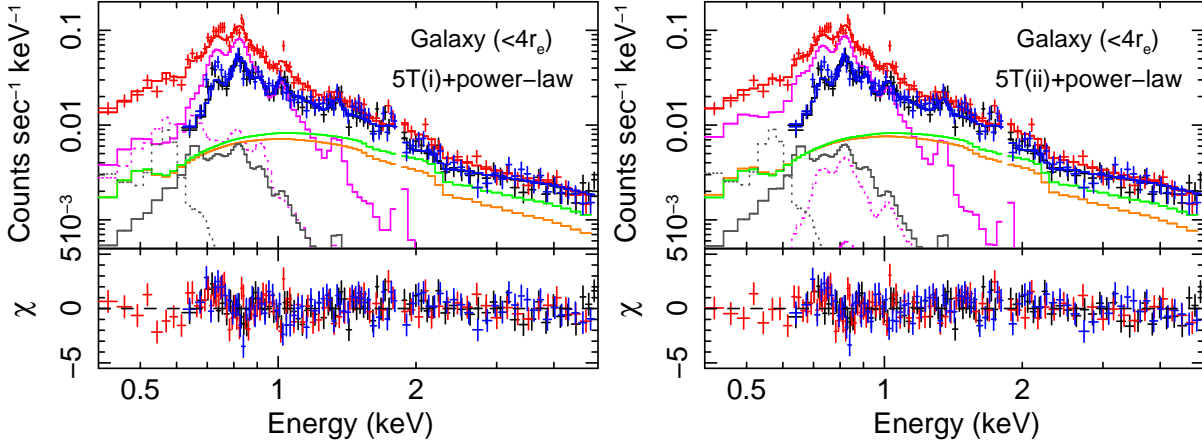


Fig. 5. Spectra within $4 r_e$ observed with XIS0 (black), XIS1 (red), and XIS3 (blue). These spectra are fitted with 5T(i)+power-law (left), and 5T(ii)+power-law (right) models. Lower panels show fit residuals. For simplicity, only model components for XIS1 spectra are shown. Colors have the same meanings as in Figure 3

Table 2. Results of spectral fittings within $4 r_e$ of NGC 4382 with 5T models

model	kT (keV)	O (solar)	Ne (solar)	Mg (solar)	Fe (solar)	χ^2 /d.o.f.
5T(i)+power-law	0.2, 0.4, 0.6, 0.8, 1.0*	$0.39^{+0.22}_{-0.15}$	$0.68^{+1.27}_{-0.32}$	$0.57^{+1.25}_{-0.29}$	$0.97^{+1.88}_{-0.40}$	783 / 655
5T(ii)+power-law	0.1, 0.2, 0.3, 0.4, 0.5*	$0.32^{+0.70}_{-0.12}$	$0.74^{+0.89}_{-0.25}$	$0.69^{+1.51}_{-0.28}$	$1.10^{+2.24}_{-0.35}$	759 / 655

*The values were fixed

model	O/Fe (solar)	Ne/Fe (solar)	Mg/Fe (solar)
5T(i)+power-law	$0.40^{+0.38}_{-0.22}$	$0.70^{+0.19}_{-0.26}$	$0.58^{+0.26}_{-0.25}$
5T(ii)+power-law	$0.30^{+0.15}_{-0.08}$	$0.67^{+0.14}_{-0.14}$	$0.63^{+0.27}_{-0.26}$

large error bars. Figure 6 shows the derived radial profiles of O/Fe, Ne/Fe, and Mg/Fe ratios. On the whole, the derived abundance ratios of the O/Fe, Ne/Fe, and Mg/Fe are consistent with those within $4 r_e$, although these ratios have large error bars. At Suzaku's angular resolution, about 30% of the photons from the luminous central region within $2 r_e$ escape into the ring of $2-4 r_e$. As a result, the derived abundance ratios of the two regions are consistent with each other. At $3-6 r_e$, the signal-to-noise ratio is not high enough to constrain the abundance pattern.

5. Discussion

5.1. Comparison with abundance patterns in the ISM of elliptical galaxies

Figure 7 shows the pattern of abundance ratios in the ISM of NGC 4382. Here, we use those derived from spectral fitting with the 1T model (Table 1). The abundance ratios of O/Fe, Ne/Fe, and Mg/Fe have subsolar values of $\sim 0.2-0.9$ in solar units. O/Fe abundance ratio is obviously smaller than those of Ne/Fe and Mg/Fe, although the values have large error bars.

Figure 7 also compares the derived abundance pattern of NGC 4382 with those of other elliptical galaxies, NGC 720 (Tawara et al. 2008), NGC 1399 and NGC

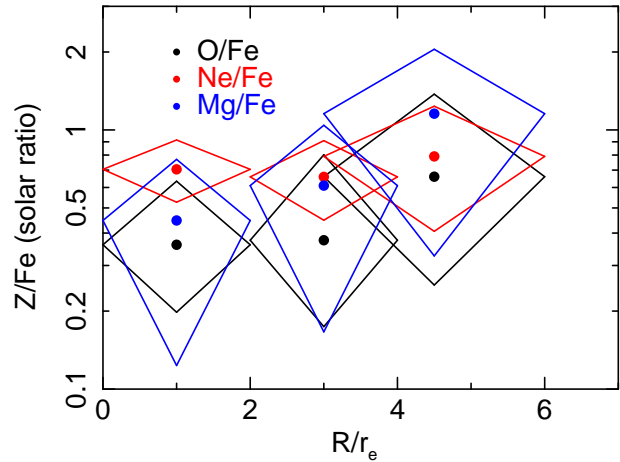


Fig. 6. Radial profiles of the abundance ratios of O, Ne, and Mg relative to the Fe abundance.

Table 3. Radial results of NGC 4382 spectral fittings

ring	model	kT (keV)	O (solar)	Ne (solar)	Mg (solar)	Fe (solar)	$\chi^2/\text{d.o.f.}$
0–2 r_e	1T+power-law	$0.318^{+0.030}_{-0.026}$	> 0.17	> 0.39	> 0.17	> 0.60	638 / 532
2–4 r_e	1T+power-law	$0.312^{+0.024}_{-0.033}$	> 0.15	> 0.30	> 0.41	> 0.49	631 / 538
3–6 r_e	1T+power-law	$0.327^{+0.044}_{-0.039}$	$0.30^{+3.13}_{-0.19}$	> 0.12	$0.52^{+5.45}_{-0.38}$	$0.45^{+10.46}_{-0.26}$	752 / 619

ring	model	O/Fe (solar)	Ne/Fe (solar)	Mg/Fe (solar)
0–2 r_e	1T+power-law	$0.36^{+0.27}_{-0.16}$	$0.70^{+0.21}_{-0.18}$	$0.45^{+0.32}_{-0.32}$
2–4 r_e	1T+power-law	$0.38^{+0.43}_{-0.20}$	$0.66^{+0.25}_{-0.21}$	$0.61^{+0.43}_{-0.44}$
3–6 r_e	1T+power-law	$0.66^{+0.71}_{-0.41}$	$0.79^{+0.44}_{-0.38}$	$1.16^{+0.89}_{-0.83}$

1404 (Matsushita et al. 2007b), and NGC 4636 (Hayashi et al. 2009). Here, the abundance values in solar units are converted using the new solar abundance table of Lodders (2003), since the other papers use different solar abundance tables, those of Feldman (1992) or Anders & Grevesse (1989). O/Fe and Ne/Fe abundance ratios increased by 60% than those adopting the solar abundances of Feldman (1992), while the Mg/Fe abundance ratio decreased by 30%, compared with that adopting the solar abundances of Anders & Grevesse (1989).

The abundance ratios of the four elliptical galaxies have a similar pattern with small scatter, except for the Ne/Fe ratios, and are not very different from the solar abundances of Lodders (2003). The average ratios of O/Fe, Ne/Fe, and Mg/Fe for these four elliptical galaxies are 0.77, 1.10, and 0.71 in solar units, respectively. As shown in Figure 7, the O/Fe ratio of NGC 4382 is smaller than those of the elliptical galaxies. Adopting the 99% confidence error, the upper O/Fe value of NGC 4382 becomes 0.61 in solar units, which is still smaller than the values of the ellipticals. The Ne/Fe ratio of the galaxy is consistent with the smallest value for the ellipticals. The uncertainty in the spectral modeling of the Fe-L lines may cause the scatter in the Ne/Fe ratio in these galaxies and also in the ICM in groups and clusters of galaxies (e.g. Matsushita 2001, Komiyama et al. 2009). The Mg/Fe ratio of the S0 galaxy has a large error and is consistent with those of the ellipticals. Since O is much more abundant in number relative to H than Ne and Mg, hereafter we will discuss possible differences in the metal enrichment histories of the ISM in NGC 4382 and the elliptical galaxies.

5.2. Contributions from SNe Ia and SNe II

The theoretical SNe Ia and SNe II yields are also plotted in Figure 7. Here, we refer to the SNe Ia yields of the W7, WDD1, and WDD3 models calculated by Iwamoto et al. (1999). The SNe II yields were taken from Nomoto et al. (2006), which is an average over the Salpeter initial mass function of stellar masses from 10 to 50 M_\odot with a progenitor metallicity of $Z = 0.02$.

The ISM abundance ratios of NGC 4382 and the elliptical galaxies are located between those of SNe Ia and SNe II. This means that the metals in the ISM are a mixture of SNe Ia and SNe II yields.

Since O is predominantly synthesized by SNe II, the observed lower O/Fe ratio in the ISM of NGC 4382 indicates larger contributions from SNe Ia to the ISM in this S0 galaxy than in elliptical galaxies. In early-type galaxies, the ISM comes from stellar mass loss and is polluted by present SNe Ia. To explain the low O/Fe ratio in NGC 4382, the present SN Ia rate may differ between NGC 4382 and elliptical galaxies, or stars in this galaxy may contain more SNe Ia products than those in elliptical galaxies.

5.3. SN Ia rate of S0 and elliptical galaxies

Assuming that the Fe abundance in the ISM is mainly the sum of stellar metallicity and the contribution from SNe Ia, it can be expressed as

$$\begin{aligned} \left(\frac{\text{Fe}}{\text{H}}\right)_{\text{ISM}} &= \left(\frac{\text{Fe}}{\text{H}}\right)_* + \left(\frac{\theta_{\text{SN}} M_{\text{SN}}^{\text{Fe}}}{\alpha_*}\right) (z_{\text{solar}}^{\text{Fe}})^{-1} \\ &= \left(\frac{\text{Fe}}{\text{H}}\right)_* + 3.5 \frac{\left(\frac{\theta_{\text{SN}}}{1.0 \times 10^{-13} \text{ yr}/L_B}\right) \left(\frac{M_{\text{SN}}^{\text{Fe}}}{0.6 M_\odot}\right)}{\left(\frac{\alpha_*}{1.5 \times 10^{-11} M_\odot/\text{yr}/L_B}\right)} \quad (\text{solar}) \quad (1) \end{aligned}$$

(see Matsushita et al. 2003 for details). Here, $(\text{Fe}/\text{H})_*$ is the stellar Fe abundance synthesized by SNe Ia, θ_{SN} is the SN Ia rate, $M_{\text{SN}}^{\text{Fe}}$ is the mass of Fe synthesized by one SN Ia, α_* is the mass loss rate of stars, and $z_{\text{solar}}^{\text{Fe}}$ is the Fe metallicity of gas with the solar abundance. Assuming the age to be 13 Gyr, we used the mass loss rate from Ciotti et al. (1991), which is approximated by $1.5 \times 10^{-11} L_B t_{15}^{-1.3} M_\odot/\text{yr}$. Here t_{15} is the age in units of 15 Gyr, and L_B is the B-band luminosity. M_{Fe} produced by one SN Ia explosion is likely to be $\sim 0.6 M_\odot$ (Iwamoto et al. 1999). Using the SN Ia rate in early-type galaxies, which was estimated to be $\sim 0.1\text{--}0.3$ SN Ia/100 yr/ $10^{10} L_\odot$ in previous studies (Crane et al. 1977; Barbon 1978; Cappellaro et al. 1997; Cappellaro et al. 1999; Turatto et al. 1999; Sharon et al. 2007; Mannucci et al. 2008), the present contribution of SNe Ia to the Fe abundance in early-type galaxies becomes 2.9–8.7 solar.

Recently, Mannucci et al. (2008) reported that the cluster membership and morphology of early-type galaxies may affect the SN rate. In clusters, the derived SN Ia rate of S0 galaxies, $0.121^{+0.097}_{-0.059}$ SN Ia/100 yr/ $10^{10} M_\odot$, tends to be higher than the $0.053^{+0.029}_{-0.020}$ SN Ia/100yr/ $10^{10} M_\odot$ of elliptical galaxies. Since the confidence level of these

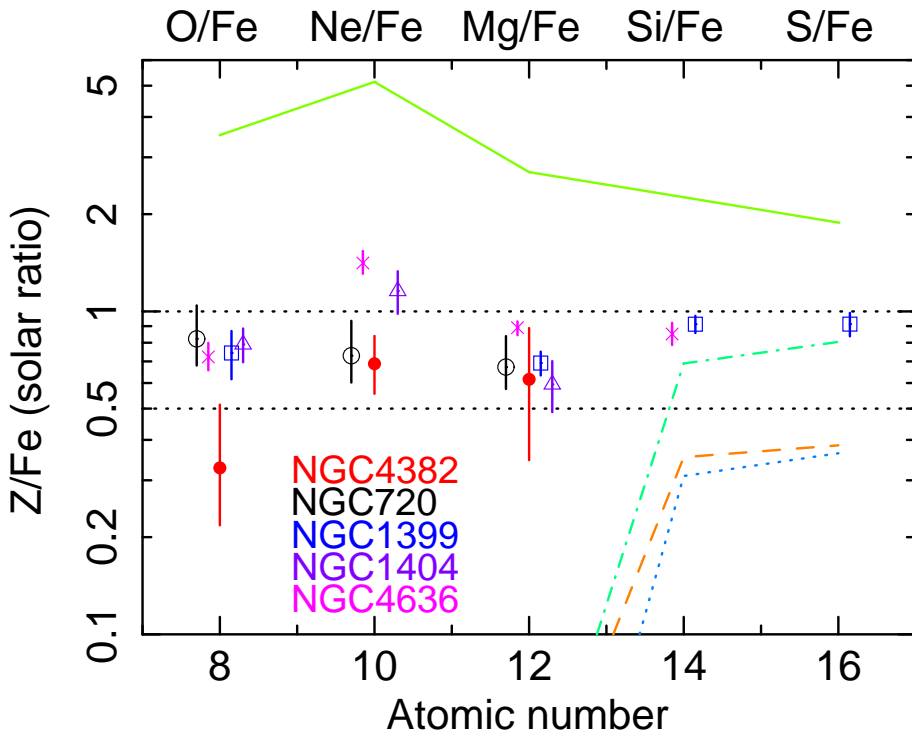


Fig. 7. Abundance ratios of O, Ne, and Mg against Fe in the ISM of NGC 4382 from the 1T model fit (filled red circles). For comparison, we plotted the abundance ratios of elliptical galaxies NGC 720 (black open circles; Tawara et al. 2008), NGC 1399 (blue open squares; Matsushita et al. 2007b), NGC 1404 (purple open triangles; Matsushita et al. 2007b), and NGC 4636 (magenta crosses; Hayashi et al. 2009). Solid line represents the abundance pattern of SNe II (Nomoto et al. 2006), and dot-dashed, dotted, and dashed lines represent those of WDD1, WDD3, and W7 of SNe Ia, respectively (Iwamoto et al. 1999).

values is 1σ , the difference is rather marginal. Assuming the stellar B-band mass-to-light ratio of NGC 4382 and the elliptical galaxies to be 3.3 and $5.0 M_{\odot}/L_{\odot}$ (Nagino & Matsushita 2009), respectively, the contributions to Fe abundance from SNe Ia in NGC 4382 and the elliptical galaxies are 5.9 – 20.9 and 4.8 – 11.9 solar, respectively. As a result of the large error bars, these values are consistent with each other.

The Fe abundances expected from the observed SN Ia rate are higher than the Fe abundances in the ISM in the early-type galaxies observed with Suzaku. This result indicates a low SN Ia rate, although the absolute values of Fe abundances have rather large errors owing to the elongated shape of the confidence contours. We note that a higher SN rate might be related to younger stellar age, in which case the stellar mass loss rate might also be higher. For example, assuming a stellar age of 10 Gyr, the mass loss rate increases by 1.4 times, and the contribution of SNe Ia to the Fe abundance decreases by 0.7 times.

5.4. Stellar O/Fe abundance ratio and evolution of S0 galaxies

The other possibility is that the lower O/Fe ratio of NGC 4382 may be because of a difference in the SN Ia products included in stars in this and the elliptical galaxies. Since a longer star-formation time scale yields more SN Ia products in stars, the difference in O/Fe ratio in stars can constrain the star-formation history. Suzaku

observes the ISM of the entire galaxy and constrains the abundance pattern in stars of the entire galaxy, while optical observations are limited to the very center.

Optical observations found higher abundances of Fe than of α -elements in stars in the central region (within 2 arcsec) of NGC 4382; $[\alpha/\text{Fe}] = 0.12 \pm 0.06$ at the 1σ confidence level (McDermid et al. 2006). Generally, giant elliptical galaxies have higher stellar abundances and higher α/Fe ratios. For example, the $[\alpha/\text{Fe}]$ of NGC 720 is 0.37 ± 0.05 within $r_e/8$ from the center of the galaxy (Humphrey et al. 2006). Therefore, the low O/Fe ratio in the ISM of NGC 4382 may reflect a lower $[\alpha/\text{Fe}]$ in stars. XMM-Newton and Chandra observations show that about half of the photons from NGC 4832 within $8 r_e$ are emitted from the region within $2 r_e$ (Nagino & Matsushita 2009). Therefore, we can conclude that at least within a few r_e the ISM shows the low O/Fe ratio. This region is much larger than that within 2 arcsec, to which the optical observations (McDermid et al. 2006) are limited. In other words, the Suzaku observations provide evidence that not only the stars in the central region of NGC 4382, but also those within at least a few r_e have a smaller α/Fe ratio than those of the four elliptical galaxies.

A number of authors found a clear correlation between the α/Fe ratio and system mass (e.g., Worthey et al. 1992; Nelan et al. 2005; Thomas et al. 2005; Graves et al. 2007). Thomas et al. (2005) found that galaxies with stellar velocity dispersion $\sigma > 200 \text{ km s}^{-1}$ have a rela-

tively higher $[\alpha/\text{Fe}]$ (> 0.2) and also have higher metallicities. NGC 4382 has a lower ISM temperature of ~ 0.3 keV, and its stellar velocity dispersion σ is 179 ± 6 km s $^{-1}$ (McDermid et al. 2006). Therefore, the lower O/Fe ratio in NGC 4382 may reflect a correlation with the system mass. Usually, these metallicity and α/Fe correlations with system mass are interpreted as showing that higher-mass systems have experienced more rapid star formation than lower-mass galaxies (e.g. Thomas et al. 2005; McDermid et al. 2006). Thus, most stars in larger systems would have formed before SNe Ia began to synthesize large amounts of Fe.

Considering the fractional evolution of S0 and spiral galaxies in clusters, spiral galaxies might have changed into S0 galaxies (e.g. Dressler et al. 1997; Fasano et al. 2000; Treu et al. 2003; Kodama et al. 2004; Postman et al. 2005; Smith et al. 2005; Desai et al. 2007; Poggianti et al. 2009). If so, stars in S0 galaxies would contain more SN Ia products than those in elliptical galaxies, reflecting the fact that stars in spiral galaxies have lower $[\alpha/\text{Fe}]$ ratios than those in giant ellipticals. For example, the value of $[\alpha/\text{Fe}]$ of the Sun is zero. If S0 galaxies in clusters generally have lower O/Fe ratios in the ISM, the hypothesis of morphology changes would be supported. To investigate further, we need more sample galaxies for which to derive abundance patterns in the ISM using Suzaku observations.

6. Summary and conclusion

With the Suzaku observation of S0 galaxy NGC 4382, we measured the ISM temperature, metal abundances of O, Ne, Mg and Fe, and their abundance ratios for the region within $4 r_e$ of the galaxy's center. The temperature, 0.3 keV, and O/Fe ratio, 0.3 in solar units, in the ISM of this galaxy are smaller than those in elliptical galaxies observed with Suzaku, NGC 720 (Tawara et al. 2008), NGC 1399 and NGC 1404 (Matsushita et al. 2007b), and NGC 4636 (Hayashi et al. 2009). The lower O/Fe ratio of the ISM may reflect a higher rate of present SN Ia or a lower α/Fe ratio in stars in NGC 4382 (McDermid et al. 2006) than in those in the four elliptical galaxies.

We thank to the referee for a careful reviewing and many helpful comments. We also thank all members of the Suzaku hardware and software teams and the science working group.

References

- Anders, E., & Grevesse, N. 1989, *Geochim. Cosmochim. Acta*, 53, 197
- Athey, A. E. 2007, arXiv:0711.0395
- Barbon, R. 1978, *AJ*, 83, 13
- Bernardi, M., et al. 2003, *AJ*, 125, 1882
- Blanton, E. L., Sarazin, C. L., & Irwin, J. A. 2001, *ApJ*, 552, 106
- Cappellaro, E., Turatto, M., Tsvetkov, D. Y., Bartunov, O. S., Pollas, C., Evans, R., & Hamuy, M. 1997, *A&A*, 322, 431
- Cappellaro, E., Evans, R., & Turatto, M. 1999, *A&A*, 351, 459
- Ciotti, L., D'Ercole, A., Pellegrini, S., & Renzini, A. 1991, *ApJ*, 376, 380
- Crane, P., Tammann, G. A., & Woltjer, L. 1977, *Nature*, 265, 124
- Desai, V., et al. 2007, *ApJ*, 660, 1151
- de Vaucouleurs, G., de Vaucouleurs, A., Corwin, H. G., Jr., Buta, R. J., Paturel, G., & Fouque, P. 1991, *Third Reference Catalogue of Bright Galaxies (RC3 Catalog)*
- Dickey, J. M., & Lockman, F. J. 1990, *ARA&A*, 28, 215
- Dressler, A., et al. 1997, *ApJ*, 490, 577
- Edvardsson, B., Andersen, J., Gustafsson, B., Lambert, D. L., Nissen, P. E., & Tomkin, J. 1993, *A&A*, 275, 101
- Fabbiano, G., Kim, D.-W., & Trinchieri, G. 1994, *ApJ*, 429, 94
- Faber, S. M., Worthey, G., & Gonzales, J. J. 1992, *The Stellar Populations of Galaxies*, 149, 255
- Fasano, G., Poggianti, B. M., Couch, W. J., Bettoni, D., Kjærgaard, P., & Moles, M. 2000, *ApJ*, 542, 673
- Feldman, U. 1992, *Phys. Scr.*, 46, 202
- Forman, W., Jones, C., & Tucker, W. 1985, *ApJ*, 293, 102
- Graves, G. J., Faber, S. M., Schiavon, R. P., & Yan, R. 2007, *ApJ*, 671, 243
- Hayashi, K., Fukazawa, Y., Tozuka, M., Nishino, S., Matsushita, K., Takei, Y., & Arnaud, K. A. 2009, *PASJ*, 61, 1185
- Humphrey, P. J., Buote, D. A., Gastaldello, F., Zappacosta, L., Bullock, J. S., Brighenti, F., & Mathews, W. G. 2006, *ApJ*, 646, 899
- Ishisaki, Y., et al. 2007, *PASJ*, 59, 113
- Irwin, J. A., Sarazin, C. L., & Bregman, J. N. 2000, *ApJ*, 544, 293
- Irwin, J. A., Athey, A. E., & Bregman, J. N. 2003, *ApJ*, 587, 356
- Iwamoto, K., Brachwitz, F., Nomoto, K., Kishimoto, N., Umeda, H., Hix, W. R., & Thielemann, F.-K. 1999, *ApJS*, 125, 439
- Kim, D.-W., Fabbiano, G., Matsumoto, H., Koyama, K., & Trinchieri, G. 1996, *ApJ*, 468, 175
- Kodama, T., et al. 2004, *MNRAS*, 350, 1005
- Komiyama, M., Sato, K., Nagino, R., Ohashi, T., & Matsushita, K. 2009, *PASJ*, 61, 337
- Konami, S., et al. 2009, *PASJ*, 61, 941
- Koyama, K., et al. 2007, *PASJ*, 59, 23
- Kushino, A., Ishisaki, Y., Morita, U., Yamasaki, N. Y., Ishida, M., Ohashi, T., & Ueda, Y. 2002, *PASJ*, 54, 327
- Lodders, K. 2003, *ApJ*, 591, 1220
- Mannucci, F., Maoz, D., Sharon, K., Botticella, M. T., Della Valle, M., Gal-Yam, A., & Panagia, N. 2008, *MNRAS*, 383, 1121
- Mathews, W. G., & Brighenti, F. 2003, *ApJ*, 599, 992
- Matsushita, K., et al. 1994, *ApJL*, 436, L41
- Matsushita, K. 2001, *ApJ*, 547, 693
- Matsushita, K., Belsole, E., Finoguenov, A., Boehringer, H. 2002, *A&A*, 386, 77
- Matsushita, K., Finoguenov, A., & Böhringer, H. 2003, *A&A*, 401, 443
- Matsushita, K., Böhringer, H., Takahashi, I., & Ikebe, Y. 2007a, *A&A*, 462, 953
- Matsushita, K., et al. 2007b, *PASJ*, 59, 327
- McDermid, R. M., et al. 2006, *MNRAS*, 373, 906
- Mitsuda, K., et al. 2007, *PASJ*, 59, 1
- Nagino, R., & Matsushita, K. 2009, *A&A*, 501, 157

- Nelan, J. E., Smith, R. J., Hudson, M. J., Wegner, G. A., Lucey, J. R., Moore, S. A. W., Quinney, S. J., & Suntzeff, N. B. 2005, *ApJ*, 632, 137
- Nomoto, K., Tominaga, N., Umeda, H., Kobayashi, C., & Maeda, K. 2006, *Nuclear Physics A*, 777, 424
- Pipino, A., Chiappini, C., Graves, G., & Matteucci, F. 2009, *MNRAS*, 396, 1151
- Poggianti, B. M., et al. 2009, *ApJL*, 697, L137
- Postman, M., et al. 2005, *ApJ*, 623, 721
- Randall, S. W., Sarazin, C. L., & Irwin, J. A. 2004, *ApJ*, 600, 729
- Sansom, A. E., O'Sullivan, E., Forbes, D. A., Proctor, R. N., & Davis, D. S. 2006, *MNRAS*, 370, 1541
- Sharon, K., Gal-Yam, A., Maoz, D., Filippenko, A. V., & Guhathakurta, P. 2007, *ApJ*, 660, 1165
- Sivakoff, G. R., Sarazin, C. L., & Irwin, J. A. 2003, *ApJ*, 599, 218
- Smith, R. K., Brickhouse, N. S., Liedahl, D. A., & Raymond, J. C. 2001, *ApJL*, 556, L91
- Smith, G. P., Treu, T., Ellis, R. S., Moran, S. M., & Dressler, A. 2005, *ApJ*, 620, 78
- Smith, R. J., Hudson, M. J., Lucey, J. R., Nelan, J. E., & Wegner, G. A. 2006, *MNRAS*, 369, 1419
- Tamura, T., Kaastra, J. S., Makishima, K., & Takahashi, I. 2003, *A&A*, 399, 497
- Tawa, N., et al. 2008, *PASJ*, 60, 11
- Tawara, Y., Matsumoto, C., Tozuka, M., Fukazawa, Y., Matsushita, K., & Anabuki, N. 2008, *PASJ*, 60, 307
- Thomas, D., Maraston, C., Bender, R., & Mendes de Oliveira, C. 2005, *ApJ*, 621, 673
- Treu, T., Ellis, R. S., Kneib, J.-P., Dressler, A., Smail, I., Czoske, O., Oemler, A., & Natarajan, P. 2003, *ApJ*, 591, 53
- Tully, R. B. 1988, *Nearby Galaxy Catalog*, Cambridge and New York, Cambridge University Press, 1988, 221 p.,
- Turatto, M., Cappellaro, E., & Petrosian, A. R. 1999, *Activity in Galaxies and Related Phenomena*, 194, 364
- Worthey, G., Faber, S. M., & Gonzalez, J. J. 1992, *ApJ*, 398, 69
- Xu, H., et al. 2002, *ApJ*, 579, 600
- Yamasaki, N. Y., Sato, K., Mitsuishi, I., & Ohashi, T. 2009, *PASJ*, 61, 291